Computers and Mathematics with Applications 61 (2011) 3564–3576

Contents lists available at ScienceDirect

Computers and Mathematics with Applications

journal homepage: www.elsevier.com/locate/camwa

Modelling of high pressure binary droplet collisions

Pablo M. Dupuy [a,*], Yi Lin [a], Maria Fernandino [b], Hugo A. Jakobsen [a], Hallvard F. Svendsen [a]

[a] Department of Chemical Engineering, Norwegian University of Science and Technology, NO-7491 Trondheim, Norway

[b] Department of Energy and Process Engineering, Norwegian University of Science and Technology, NO-7491 Trondheim, Norway

ARTICLE INFO

Article history:
Received 15 October 2009
Received in revised form 26 May 2010
Accepted 30 May 2010

Keywords:
Low Weber number collisions
Two-phase flow
Diffuse interface model
Droplet–droplet collisions

ABSTRACT

Droplet collision efficiency is a rather uncharted area for real hydrocarbon systems under non-atmospheric conditions. It is also of great interest in many industrial applications. In this work binary head-on droplet collisions at high pressure have been simulated using the lattice Boltzmann method. A model that captures the physics of the coalescence process is used where no external criterion for coalescence is needed. The collision process is described in terms of hydrodynamic variables and through a quantitative study of energy loss. At high pressures, low inertia collisions are the most frequent. Distinguishing between bouncing and coalescence under these conditions is needed in order to provide closure conditions for macroscopic CFD models. A limit of $Re < 170\sqrt{\rho_{lg}}$ is found to predict coalescence in all the cases simulated. In addition this paper explains the stochastic behaviour of low inertia coalescence at high pressure. This has major implications both when building macroscopic models for predicting industrial process efficiencies and in the optimization of equipment internals working with droplets at high pressure as is the case for combustion chambers and gas–liquid separators.

1. Introduction

Separation in high pressure gas–liquid hydrocarbon systems represents a topic of interest in many fields of engineering. An example is in liquid-in-gas flows, where all the liquid is to be removed through processes of droplet collisions with droplets, walls and liquid surfaces. Thorough experimental investigations in these systems are very difficult as the following challenges are among those that have to be taken into account: explosion risk, properties dependent on conditions of equilibrium between the two phases, mixtures with near critical point behaviour and increased density of the gas phase.

Extensive experimental work has been carried out in the past, where general collision maps were developed [1–3]. These defined the following regions: high Weber number coalescence, low Weber number coalescence, bouncing, stretching and reflexive separation. In Fig. 1 these regimes are sketched as a function of the off-centre impact parameter B and the Weber number (We). The Weber number is defined as $\frac{\rho_h u^2 D}{\sigma}$, with ρ_h being the liquid density, u the droplet velocity relative to the centre of mass, D the characteristic droplet size and σ the interfacial tension. These maps are specific for each experimental configuration, and are unique for each chemical system and cannot be extrapolated to other conditions. This implies that new experiments must be conducted for all new systems. In order to generalize the results the boundaries between regimes are parametrized as functions of system properties and the experimental configuration.

The Weber number as a characterizing parameter has almost exclusively been used in the literature due to good results at high inertia and because most of the previous work makes reference to one of the pioneering works in the field that study the air–water system at atmospheric conditions [1]. The low inertia coalescence regime, highlighted in the work of Qian and

* Corresponding author.
E-mail addresses: dupuy@nt.ntnu.no, dupuypablo@gmail.com, pablo.dupuy@nt.ntnu.no (P.M. Dupuy), maria.fernandino@nt.ntnu.no (M. Fernandino).

0898-1221/$ – see front matter © 2010 Elsevier Ltd. All rights reserved.
doi:10.1016/j.camwa.2010.05.044

Nomenclature

$\hat{D}$ (D) real (simulation) droplet size.
t *lattice time*, simulation time equal to the time taken for a pseudo-particle to travel from a lattice node to the adjacent node.
$\hat{t}$ *time* (s), real time.
$\tilde{t} = \frac{\hat{t}\hat{L}}{\hat{V}} = \frac{tL}{V}$ *normalized time*.
$\hat{L}$ (L) real (simulation) semi-distance between droplets.
$\hat{V}$ (V) real (simulation) initial velocity of a droplet to the centre of mass of the system.
$\tilde{K} = \frac{\hat{K}}{\hat{K}_0} = \frac{K}{K_0}$ normalized relative energy.
CT coalescence time.
IFE interfacial free energy.
ICT inverse coalescence time.
M mobility [19].
$vc = \frac{\mu_{\mathrm{LB}}}{\mu}$ viscosity correction ratio [4].
$\rho_{lg} = \frac{\rho_l}{\rho_g}$ liquid to gas density ratio.
$Re = \frac{\rho_l DV}{\mu_g}$ Reynolds, droplet inertia vs. gas viscosity.
$Re_{\mathrm{liq.}} = \frac{\rho_l DV}{\mu_l}$ Liquid Reynolds, droplet inertia vs. liquid viscosity.

Law [2], is not necessarily best represented in terms of We. This may be irrelevant if the only parameters that are changed are the droplet size and velocity. But the question is that of how we can improve our understanding at other pressures such as in the high pressure range up to 100 bar and beyond. We propose investigating how the energy of a binary collision system changes from one regime to another while changing pressure.

Under atmospheric conditions, particularly when working with hydrocarbon systems, the distinction between bouncing and coalescence is trivial [1]. At low velocities (i.e. low Reynolds and Weber numbers), bouncing is observed when there is not enough inertia for the interdroplet gas to drain out. At higher pressures and with hydrocarbon systems, coalescence is observed in the very low inertia region instead of bouncing. At the moment, it is not completely understood how to model this since other forces are involved, not only hydrodynamics [2]. At higher pressures the plastic component of the collision becomes dominant over the elastic one. This predicts that the rebound velocity with respect to the centre of mass is reduced with increasing pressure. This opens a new range of coalescence possibilities which are not present under atmospheric conditions. The phenomena that follow are complex, and an investigation of the process for different ambient pressures requires simplifications. We model the interface physics using the gradient theory in order to have a model which has the coalescence mechanisms embedded. The influence of the interface mobility is not studied in the present work; rather it is concerned with how the collision outcomes vary with the hydrodynamic parameters at different pressures.

The boundary between low Weber number coalescence (with immediate and retarded coalescence regimes) and bouncing is studied by using model simulations. The model is solved by the lattice Boltzmann method. This method is presented bearing in mind that the behaviour of the stress tensor along the gas–liquid interface can be adjusted by means of the fractional step [4]. This will show how pseudo-fluid solvers such as the lattice Boltzmann one can be used for real fluid applications.

In the next section the model is described, together with the method and implementation details. Section 3 is dedicated to the energy equations used to study the droplet collisions. Section 4 shows the conditions of the real industrial case and how to model collisions under these conditions. The results are examined in Section 5 and the analyses and discussions are presented in Section 6. The work is concluded in Section 7 which highlights the new findings.

2. The model

Mathematical and numerical models are developed in order to predict whether coalescence, bouncing or separation occur for a given system and geometry. This is based on dimensionless parameters such as the density and viscosity ratios, Reynolds and Weber numbers, geometrical parameters, and other properties of the system. Using the lattice Boltzmann (LB) method, many models for phase separation simulations can be found. Both one-component gas/liquid and binary fluid system models are presented in the literature [5–14]. Some two-phase flow models incorporate an interparticle potential [6,7]. Models based on kinetic theory have been used for gas mixtures [15] and were further developed in the last decade [16,17].

We follow the free energy approach since it has shown its potential for working at high density ratios (ρ_{lg}) and eliminating spurious numerical currents. This approach is also used because we need a consistent model of interfacial physics. The following macroscopic single-field formulation is indirectly solved [18]:

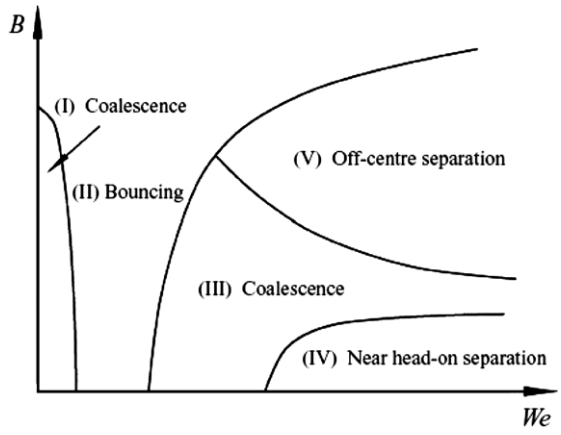

Fig. 1. Various collision regimes of hydrocarbon droplets.
Source: (Extracted from Ref. [2].).

$$\frac{D\phi}{Dt} + \vec{u} \cdot \nabla\phi = M\nabla^2\mu_\phi \tag{1}$$

$$\frac{D\delta p}{Dt} + \rho_\phi \frac{\mathrm{d}\mathcal{P}}{\mathrm{d}\rho}\nabla \cdot \vec{u} = 0 \tag{2}$$

$$\rho_\phi \frac{D\vec{u}}{Dt} + \rho_\phi \vec{u} \cdot \nabla\vec{u} = -\nabla\delta p - \rho_\phi \nabla\mu_\phi + \nabla \cdot \mathcal{T} \tag{3}$$

where $\vec{u}$ is the flow velocity vector, δp is the perturbed pressure component, $\frac{\mathrm{d}\mathcal{P}}{\mathrm{d}\rho}$ is the compressibility, $\mathcal{T}$ is the viscous stress tensor, M is the Cahn–Hilliard mobility [19], and μ_ϕ is the chemical potential. The mobility is the constant of proportionality between the concentration flux and the gradients of chemical potential. For a binary gas–liquid system it is directly related to the diffusion coefficient and the temperature. If the density is expressed in $\mathrm{kg/m^3}$, the units of the mobility are $\mathrm{kg^2/(ms\,J)}$. The reference component density, ρ_ϕ, is calculated through an order parameter, defined as $\phi = \rho_\phi - 0.5(\rho_g + \rho_l)$, according to [18], which is consistent with this work as regards nomenclature. Eq. (1), the so called phase-field equation, describes the convection of density and the variations due to diffusion. Eq. (2) is the compressibility equation, where these variations in pressure will enforce the fluid flow but will not affect the density of the system. Eq. (3) is the momentum balance.

As proposed by Cahn and Hilliard [20], the Helmholtz free energy can be written as

$$\Psi : \Psi_\rho(\rho, \nabla\rho) = \Psi_\phi(\phi, \nabla\phi) = \overbrace{A(\phi + \phi^*)^2(\phi - \phi^*)^2}^{\Psi_0} + \frac{\kappa}{2}|\vec{\nabla}\phi|^2. \tag{4}$$

It is comprised of two terms. The first (Ψ_0) is given by the equation of state and represents the excess free energy, while the second is a non-local contribution of extra free energy associated with the interactions between molecules and their surrounding molecules in a non-homogeneous fluid.

This is used to define the chemical potential $\mu_\phi = \frac{\partial\Psi_0}{\partial\phi} - \kappa\nabla^2\phi$. No temperature dependent term is explicitly added in the internal energy formulation since the temperature changes are not simulated.

2.1. The solution method

The present section details the method used for solving the present model.

Eq. (3) is split by an operator splitting technique [4] where

$$\int_t^{t^*} \frac{\partial\vec{u}}{\partial t}\mathrm{d}t = \int_t^{t^*} \left(-\vec{u} \cdot \nabla\vec{u} - \frac{1}{\rho}\nabla\delta p + \frac{1}{\rho}\nabla \cdot \mathcal{T}_{\mathrm{LB}} - \nabla\mu_\phi\right)\mathrm{d}t \tag{5}$$

is solved using the lattice Boltzmann method and

$$\int_{t^*}^{t^+} \frac{\partial\vec{u}}{\partial t}\mathrm{d}t = \int_{t^*}^{t^+} \left(\frac{1}{\rho}\nabla(\mathcal{T} - \mathcal{T}_{\mathrm{LB}})\right)\mathrm{d}t \tag{6}$$

is solved using finite differences as an extra step. The operator splitting technique was first applied to lattice Boltzmann problems by Shu et al. [21].

The two lattice Boltzmann distribution function equations are given by

$$\hat{f}^{t+1}_{i,x+e} = {}^{\mathrm{eq}}f^{t}_{i,x} + \frac{1}{2}({}^{\mathrm{ITF}}\mathcal{F}^{t}_{i,x} + {}^{\mathrm{DP}}\mathcal{F}^{t}_{i,x}) \qquad D2Q9 \tag{7}$$

$$g^{t+1}_{i,x+e} = g^{t}_{i,x} + \left[1 - \frac{2}{2\tau_g + 1}\right](g^{t}_{i,x+e} - g^{t}_{i,x}) + \Omega_i g \;\; D2Q5. \tag{8}$$

Here $f^t_{i,x}$ is the ith density function (or pseudo-particle) at node x at time t, and $\vec{e}_i$ is the discrete velocity vector of pseudo-particle i. The first equation gives the distribution f for the calculation of the momentum and perturbed pressure component and the second gives the distribution g for the density. It is assumed that $\vec{u}\cdot\nabla\delta p$ is of order u^3 and that the lattice Boltzmann speed of sound is used everywhere in the domain as in [22]. The Crank–Nicholson approach introduces two steps for the streaming and collision of the density function, where $\hat{f}$ is a temporal variable that in the normal procedure for any relaxation time [22] is used for calculation of both the moments and the post-collision density distribution. In our approach, a fixed relaxation time of 1/2 is chosen (note that this is stable [22]). This means that the temporal variable $\hat{f}$ is only needed for calculation of the moments. The extra step required by the Crank–Nicholson approach [22] is replaced by one extra fractional step for correction of the viscosity with the advantages and disadvantages discussed in the literature [4].

The equilibrium distribution is calculated from the hydrodynamic moments

$${}^{\mathrm{eq}}f_i = 3\delta p w_i + \rho_\phi \mathcal{V}_i(\vec{u}), \tag{9}$$

$$\mathcal{V}_i(\vec{u}) = w_i\left(3e_{i,\alpha}u_\alpha - \frac{3}{2}u^2 + \frac{9}{2}u_\alpha u_\beta e_{i,\alpha}e_{i,\beta}\right), \tag{10}$$

where the Greek letters in subscripts correspond to the Cartesian coordinate directions in which the Einstein summation convention is used. For the density equilibrium distribution we define

$${}^{\mathrm{eq}}g_i = -2\Gamma\mu_\phi + \phi \quad i = 1 \tag{11}$$

$${}^{\mathrm{eq}}g_i = \frac{1}{2}\Gamma\mu_\phi + \frac{1}{2q}\phi e_{i,\alpha}u_\alpha \quad \forall i \in [2,5]$$

where the parameter Γ is defined via the Cahn–Hilliard mobility, $M = \Gamma q(\tau_g q - 0.5) = \Gamma\frac{2\tau_g - 1}{(1+2\tau_g)^2}$, with $q = (\tau_g + 0.5)^{-1}$. From the moments of g and $\hat{f}$ it is possible to calculate the fluid variables:

$$\delta p = \frac{1}{3}\sum_i \hat{f}_i + \frac{1}{2}\vec{u}\cdot\nabla\phi \tag{12}$$

$$\rho_\phi\vec{u} = \sum_i \hat{f}_i\vec{e}_i + \frac{1}{2}\mu_\phi\nabla\phi \tag{13}$$

$$\phi = \sum_i g_i. \tag{14}$$

Two force terms are necessary for the density–pressure decoupling (DP) and the interfacial tension forces (ITF) [18]:

$${}^{\mathrm{DP}}\mathcal{F}_i = (\vec{e}_i - \vec{u})\cdot\nabla\rho_\phi\mathcal{V}(\vec{u}) \tag{15}$$

and

$$\Phi = \phi\mu_\phi + \delta p \tag{16}$$

$$\mathcal{A}_i = \frac{27}{4}\delta p - \frac{15}{4}\Phi \quad i = 1 \tag{17}$$

$$\mathcal{A}_i = 3\Phi \quad \forall i \in [2,9] \tag{18}$$

$${}^{\mathrm{eq}}f_i = \mathcal{A}_i w_i + \rho_\phi\mathcal{V}_i(\vec{u}) \tag{19}$$

$${}^{\mathrm{ITF}}\mathcal{F}_i = \frac{(\vec{e}_i - \vec{u})}{c_s^2}\cdot\mu_\phi\nabla\phi(w_i + \mathcal{V}(\vec{u})). \tag{20}$$

The differentials of the chemical potential are not needed, while the differential of the product $\phi\mu_\phi$ is implicitly calculated by using the lattice Boltzmann scheme. The only gradients needed explicitly are those of the density. The term $\vec{e}_i\cdot\nabla\rho_\phi$ is computed using the *second-order biased differences* according to [22].

3. Conservation of energy

The conservation of total energy is expressed by the first law of thermodynamics. The energy balance relates work and heat to the internal energy, kinetic energy, and potential energy of the closed system:

$$dE_{\text{total}} = d(\Psi + K + E_p) = \delta Q + \delta W \tag{21}$$

where Ψ, K and E_p are the intensive internal, kinetic and potential energies of the centre of mass of the system. In the above equation, the symbol d indicates a differential element of a state function, and the symbol δ indicates a differential element of some quantity which is not a state function [23].

The kinetic energy equation is obtained as

$$\begin{aligned}\frac{\partial K}{\partial t} &= \frac{\partial}{\partial t}\left(\rho\frac{1}{2}v^2\right)\\ &= -\nabla\cdot\left(\rho\frac{1}{2}v^2\vec{v}\right) - \nabla\cdot(p\vec{v}) + p(\nabla\cdot\vec{v}) - \nabla\cdot[\sigma\cdot\vec{v}] + \sigma : \nabla\vec{v} - \frac{\partial\Psi}{\partial t} + \vec{v}\cdot\sum_{c=1}^{N}\rho_c\vec{v}_{c,d}\Phi_c\end{aligned} \tag{22}$$

where in general the i-th term is denoted as $\frac{\partial K}{\partial t}_i$. The integration of Eq. (21) over phases and the entire domain is used to track the balances between different energies during the simulation. In addition, spatial integrated values of the terms on the right-hand side (RHS) of Eq. (22) are plotted sharing the same axes. Here, the following will be non-trivial for the model problem: the third term on the RHS, denoting the rate of reversible conversion of the kinetic energy to internal energy, the fifth term on the RHS, denoting the rate of irreversible conversion of kinetic energy to internal energy, and the sixth term on the RHS, denoting the rate of release of internal energy. Note that neither potential energy nor temperature variations are considered in the present work.

4. Modelling for scrubber conditions

4.1. Dimensional analysis

The physical space is transformed to a dimensionless space. Any arbitrary real distance, such as the half-distance between droplets, $\hat{L}$, is normalized with the real droplet diameter $\tilde{L} = \hat{L}/\hat{D}$. Any time from the physical domain, $\hat{t}$, is normalized by incorporating the droplet velocity, $\hat{V}$, and a characteristic length: $\tilde{t} = \hat{t}\hat{L}/\hat{V}$. Physical domain densities, $\hat{\rho}$, are normalized with respect to the gas density $\tilde{\rho} = \hat{\rho}/\hat{\rho}_g$. Having defined time, space, and mass, the domain can be transformed to any other domain, such as the lattice Boltzmann dimensionless domain. For example converting a time from the lattice Boltzmann results to the physical domain can be done by using $\hat{t} = \frac{\hat{V}}{V}\frac{L}{\hat{L}}t$, where t, V and L are in lattice Boltzmann units.

4.2. Information from the physical domain

The simulation domain is a gas space with two identical droplets placed on two sides of the domain. The domain is symmetrical along both the x-axis and the y-axis. All information needed is therefore from one quarter of the domain. The model calculates and stores this information from one quarter of the domain, since only head-on collisions are studied here.

For non-negligible gas densities there is a significant interchange of momentum between droplets and the gas phase. The approaching velocity concept needs to be redefined at high pressures. The reference velocity (so-called initial velocity when working at atmospheric conditions), which is used for defining the dimensionless numbers, is the threshold velocity used to stop the head-on acceleration process. This is designated as V. The *initial* kinetic energy of the droplet (K_0) can be calculated on the basis of this velocity, and is used for normalization of all the energy plots presented in this work. However, the entire mechanical energy of the system at an instant after the droplet is released by the acceleration field is greater than this value since the gas has a non-negligible kinetic energy.

When using a pseudo-fluid solver, there is a requirement to transform input data from the real gas–liquid system in a subsea separator to a lattice Boltzmann data system. This is a common procedure for lattice Boltzmann use and it is explained below how the real physical data are introduced into the pseudo-fluid solver.

Parameters such as the droplet size (diameter) and initial velocity, gas and liquid phase viscosities and interfacial tension need to be transformed into a scale that works in the simulation domain. Under the transformation a similitude concept is applied. However, the dimensionless numbers such as the Weber and Reynolds numbers have not been changed. These dimensionless numbers are bridges between the real liquid–gas system in a scrubber and the lattice Boltzmann model. A schematic graph of the transformation steps is shown in Fig. 2.

There are certain limitations for the ranges of values that must be taken into consideration. Velocities cannot be close to the speed of sound due to lattice Boltzmann method limitations. In order to avoid high velocities in the gas drain process the maximum initial velocity was set to $V = 0.004$. The viscosity correction ratio $\left(vc = \frac{\mu_{LB}}{\mu}\right)$ should be below 100 in the fractional step, Eq. (6). A high correction value ($\gg$100) creates a risk of returning non-physical simulation outcomes [4].

It should be mentioned that in this model, pressure itself does not appear explicitly in any of the equations. Here the pressure has no direct effect on the simulations. However, some of the other fluid properties depend on the pressure, e.g. gas density and interfacial tension. Thus pressure has indirect non-linear effects on the simulation outcome. Note that the fluctuating pressure in Eq. (2) is several orders of magnitude smaller than the thermodynamic pressure as discussed in [18].

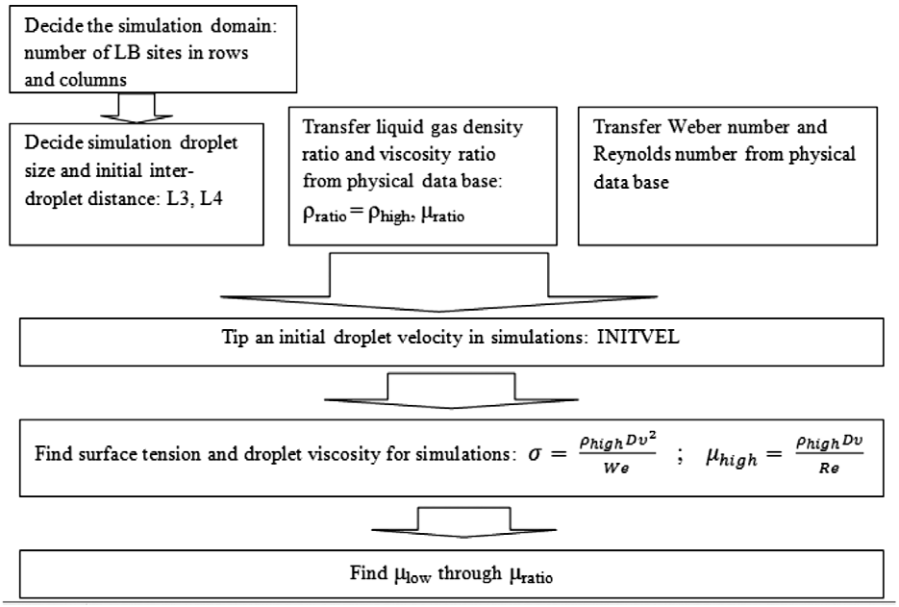

Fig. 2. Description of the data transformation.

Table 1
Physical properties of industrial interest.

Pressure (bar)	$\hat{\rho}_{liq}$ (kg/m^3)	$\hat{\rho}_{gas}$ (kg/m^3)	$\hat{\mu}_{liq}$ (mPa s)	$\hat{\mu}_{gas}$ (mPa s)	ITF (mN/m)
80	690.0	68.78	0.315	0.0137	8.668
100	678.2	89.85	0.292	0.0148	7.158
130	661.1	122.5	0.268	0.0168	5.338
150	654.0	144.6	0.257	0.0184	4.393

Table 2
Simulation parameters. The initial distance between the droplets (L) is 102, droplet diameter (D) is 120 and reference velocity $V = 0.004$.

We	0.60	0.99	0.21	0.95	1.06	1.47	1.20	1.40	1.39	1.79
P [bar]	80	80	100	100	100	100	120	120	150	150
vc_{gas}[a]	15	19	9	20	21	25	24	26	26	29
vc_{liq}[b]	6.5	8.4	3.9	8.3	8.7	10	8.3	9.0	8.5	9.6
M[c] 10^{-03}	0.086	0.049	0.24	0.053	0.048	0.034	0.045	0.039	0.041	0.031

[a] Viscosity correction ratio for the gas phase, Eq. (6).
[b] Viscosity correction ratio for the liquid phase, Eq. (6).
[c] Mobility, Eq. (1).

The real physical properties used in this work are summarized in Table 1. The interfacial tension data were calculated using gradient theory. The rest of the data were obtained from Hysys simulations. The data used in the lattice Boltzmann simulations are shown in Table 2.

5. Collision results

5.1. From bouncing to coalescence

When two droplets of identical characteristics approach each other the continuum theory cannot be used to explain how the centre point of the system gradually turns from gas to liquid, i.e. the coalescence process. Thus, continuum theory predicts an extremely thin, but finite, gas film trapped between the two droplets during the whole collision process, always resulting in bouncing as the collision outcome. However, this picture is not the case in reality. Either the continuity is broken at molecular order scales or the symmetry is broken due to small natural perturbations. How thin the film is and for how long it remains at such a reduced thickness will compete directly with the dynamics of the film rupture process. The pre-set threshold limit normally used as a coalescence criterion is in this work replaced by a model that is capable of capturing the intrinsic dynamics of the droplet interface with its own time characteristics. When decreasing the relative droplet velocity, the bouncing cases predicted by the continuum theory start to show coalescence at later times. This is called retarded coalescence. Fig. 3 presents a retarded coalescence case. The entire initial kinetic energy is dissipated in a

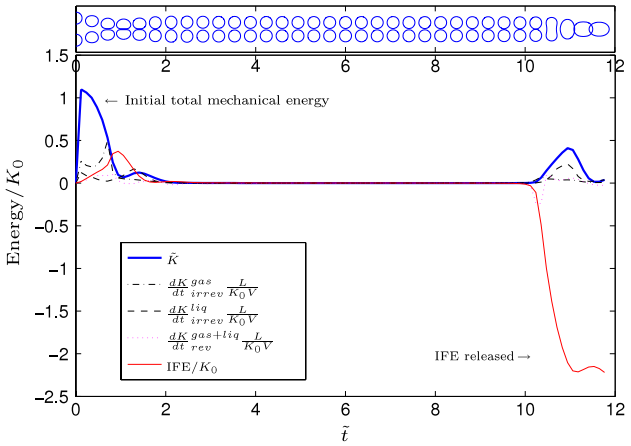

Fig. 3. Retarded coalescence. Plastic collision in the first transient. The interfacial free energy (IFE) is released when coalescence occurs.

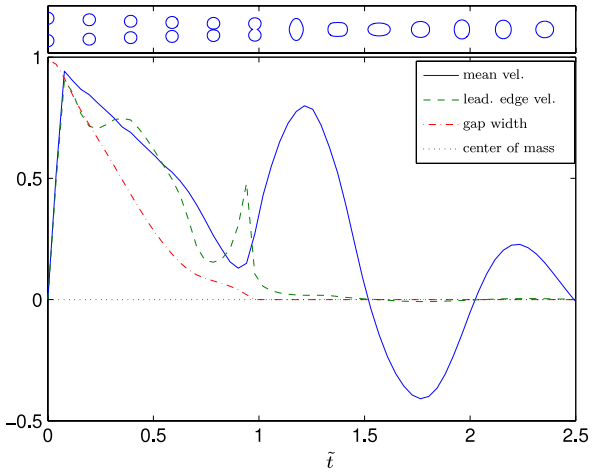

Fig. 4. Velocities and gas gap width for a coalescence case.

plastic collision shortly after $\tilde{t} = 1$. Later ($\tilde{t} = 9$), interfacial free energy (IFE) is liberated in the coalescence process and the fluid is accelerated into one coalesced droplet. The energy loss corresponds to the variation of the sum of the energy terms, where the dissipation is read as its slope. Note that the excess free energy definition, Eq. (4), has an arbitrarily associated constant. As the initial energy of the system is defined as zero the final coalesced system has a lower, and thus negative, energy.

Fig. 3 shows the energy variation of the retarded collision case. The time is made dimensionless by dividing by the collision time as if the gas phase was not present. It is shown that coalescence does not appear until after 10 times the expected collision time. The retarded coalescence event moves closer to the collision instant when the initial velocity is reduced further.

The present work considers results for collision between two-dimensional droplets. The gas can escape more easily in the three-dimensional case compared with the present case. This is expected to increase the probability for coalescence rather than bouncing. On the other hand, the case of one droplet interacting with a flat liquid film will present similarities with a different symmetry, placed between the two cases. The two-dimensional case is the simplest, and is thus studied first so that the process can be explained in qualitative terms.

In order to characterize the collision process we draw attention to the internal mechanisms present in both coalescence and bouncing simulations. We give first a description of each regime.

5.2. Coalescence simulation

A coalescence case is presented with these simulated conditions: pressure of 100 bar, Weber number of 0.2, and Reynolds number of 222 (liquid Reynolds number of 11).

The minimum distance between the two droplets is measured and plotted. Fig. 4 illustrates the situation when the distance reaches zero, i.e. the moment when the two droplets start to touch each other. Two velocities are also plotted

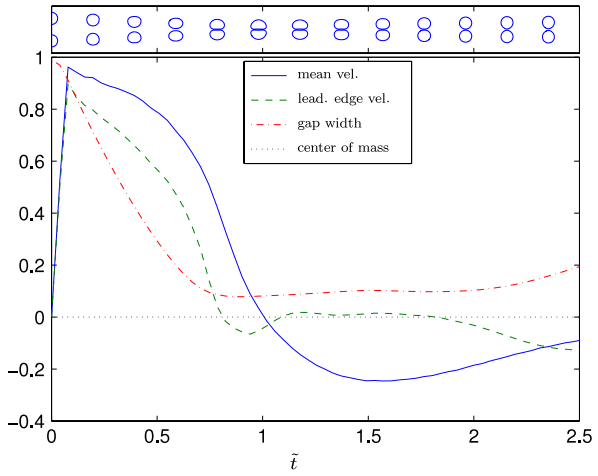

Fig. 5. Velocities and gas gap width for a bouncing case.

together in Fig. 4. The mean velocity of the droplets is always positive, and is calculated as the mean velocity of the liquid over half the domain. The velocity of the leading edge of the droplet is also shown. Both velocities are defined for the two-droplet system. It is remarkable that the edge velocity oscillates over and below the mean droplet velocity. It means that the edge moves forwards and backwards with respect to the droplet. It moves backwards due to a natural deformation of the droplet produced by the resistance of the gas gap. The edge velocity reaches a maximum just prior to coalescence. This is triggered by the film rupture process as modelled in [18]. The rest of the remaining liquid fluid that corresponded to the droplet is further accelerated due to the curvature inversion around the contact neck. After coalescence the edge velocity is interpreted as the velocity near the centre of the resulting droplet becoming zero. For the mean half-droplet velocity, the plots are continued even after coalescence to give an idea of the oscillations produced after coalescence. If the coalescence occurs in the vicinity of $\tilde{t} = 1$ the coalescence process corresponds to a normal coalescence regime reported in the literature [1].

5.3. Bouncing simulation

A bounce back case distinguishes itself from the coalescence case in many ways. The differences in the physical process and energy dissipation between bouncing and coalescence are presented in this section. An example from the droplet–droplet bouncing cases is chosen here. The simulation conditions are: pressure of 100 bar, Weber number of 1.4, and Reynolds number of 588 (liquid Reynolds number of 28).

Fig. 5 shows how the interdroplet distance, or gap width, reaches a minimum. Some instants after this minimum is reached first the edge velocity and then the mean droplet velocity become negative. At this point both droplets have started to bounce back. But at the same time during the range of approximately $\tilde{t} = (1 \ldots 2)$ the leading edge moves forwards slowly. This is evidence that the interdroplet gas gap is small enough to allow the diffusion process to start. Nevertheless this gap is large enough and if the droplets have enough kinetic energy they will separate again, far enough to avoid any possibility of retarded coalescence.

5.4. Retarded coalescence simulation

This regime belongs among the coalescence regimes but can be seen as a transition regime as well, making it difficult to define any sharp boundary between regimes. Retarded coalescence occurs for $\tilde{t} \gg 1$ and is responsible for giving the collision process stochastic behaviour also during the long time needed for retarded coalescence to take place; any external disturbance which is easily produced by turbulence will enhance or prevent coalescence.

Fig. 6 shows how the interdroplet distance reaches a local minimum; it stays in this plateau until it reaches a new minimum just before bouncing, and this reaches a maximum, and then evolves slowly towards coalescence. This case does not present significant differences from the bouncing case. But the dynamics for diffusion and bouncing back are such that the diffusion process is not stopped and finally it triggers coalescence. During $\tilde{t} = (3 \ldots 10)$ the leading edge velocity is never negative, as is shown in Fig. 6. Note that the local minimum observed prior to bouncing, around $\tilde{t} = 2$, correlates with the tail reported in Figure 3 in [24].

6. Analysis

Fig. 7 shows four cases at an ambient pressure of 100 bar. For a Weber number of 0.2 early and evident coalescence is observed around the expected contact time. Oscillations after the coalescence can be seen from the wide amplitude

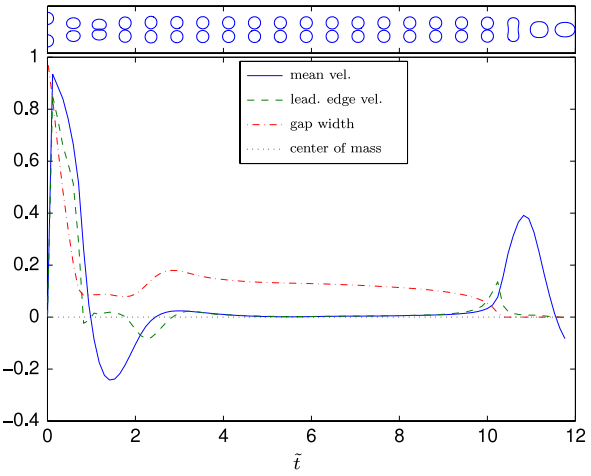

Fig. 6. Velocities and the gas gap width for a retarded coalescence case (with coalescence dimensionless time $\gg 1$).

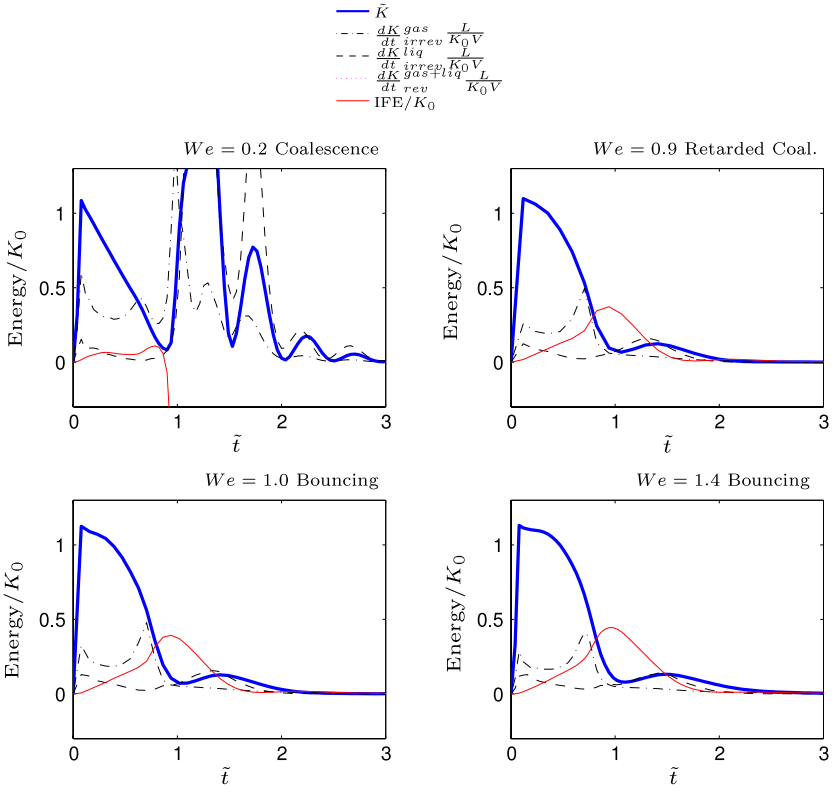

Fig. 7. Energy plot for the first transient of four collisions at 100 bar. The first two cases correspond to coalescence and retarded coalescence. The last two are bouncing cases.

variations for the kinetic energy. The next three cases with a non-uniform increasing Weber number look very similar and they correspond to retarded coalescence and two bouncing cases respectively. Energy dissipation is plotted together with energy levels where the normalization time is used to match the units. It is notable that the viscous dissipation in the gas phase is greater than in the liquid phase while the viscosity coefficients present the opposite relationship. Remarkably, most coalescence maps are drawn using a Reynolds number defined with the liquid viscosity. Furthermore, this difference is more accentuated at lower Weber or Reynolds numbers. The viscous gas dissipation has approximately twice the effect in the lower We cases compared to the situation at higher Weber numbers. This difference is not as strong for the liquid phase.

Fig. 7 also shows the deformation energy, measured as interfacial free energy (IFE). The coalescence at low Weber numbers is produced with a minimum of deformation. In contrast, the deformation energy is maximum for the high Weber

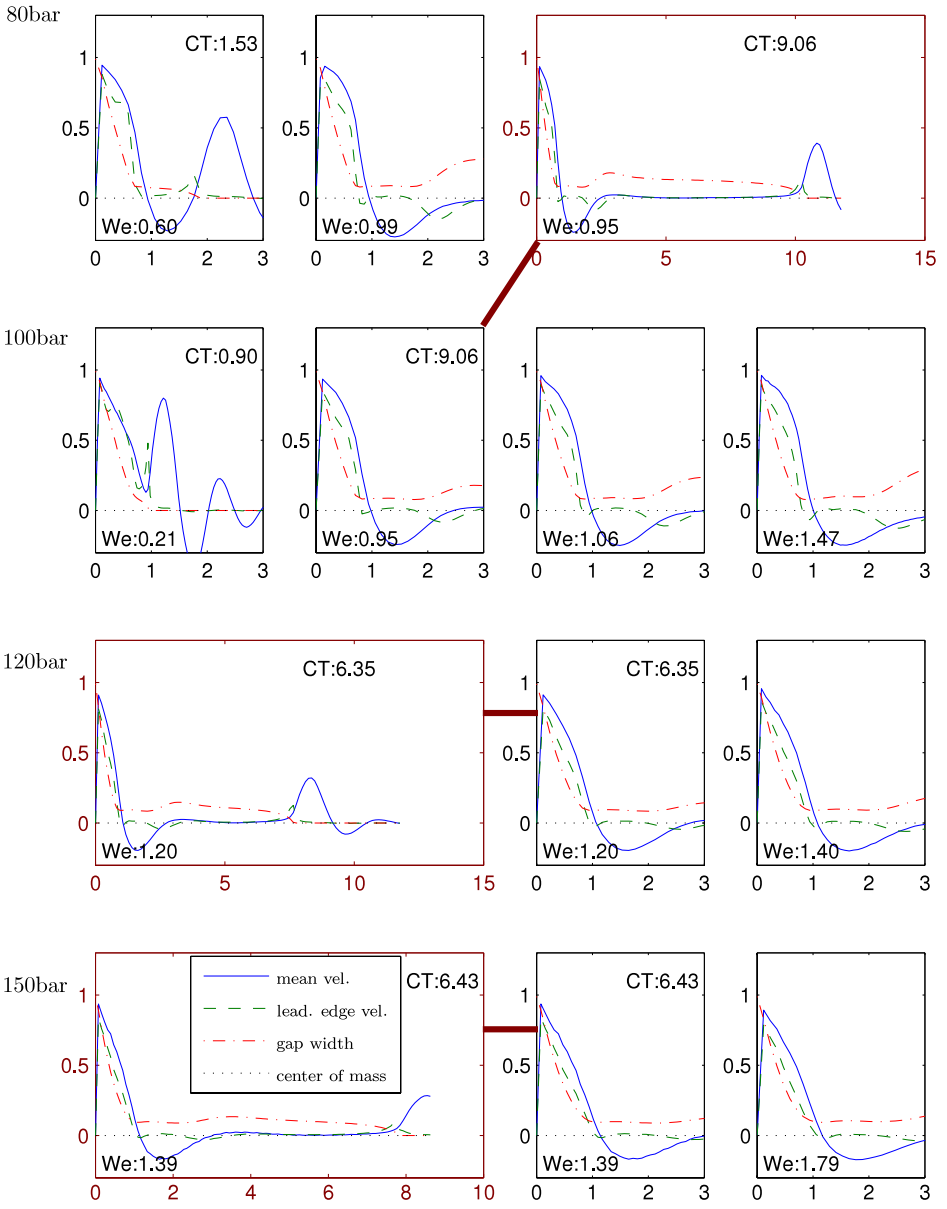

Fig. 8. Velocity and gas gap for all simulated cases ordered by ambient pressure and Weber number. The upper right-hand corner numbers correspond to dimensionless coalescence time. Plots without this time resulted in bouncing.

number case. This may seem contradictory at first sight as the higher the Weber number, the lower the interfacial energy of the droplet compared to its inertia. However, in all the cases shown in Fig. 7 this energy is below half of the initial kinetic energy of the droplet. The kinetic energy is temporarily stored in the form of interfacial deformation. For lower interfacial tensions, higher deformations are expected. The fact that not only greater deformations, but also greater deformation energies are observed when increasing the Weber number is explained by an increase in the Reynolds number.

All the simulated cases are plotted together in Fig. 8. The dimensionless time at which coalescence begins is written in the upper right-hand corner of each graph. Observations similar to those made in the previous section are valid here. The graphs are ordered by pressure and Weber number. All the cases simulated corresponding to the same observations are in perfect agreement with those pointed out in Section 5.

The plots of the various energy terms for all the cases are grouped in Fig. 9, following the same structure as Fig. 8. In addition, multimedia files can be seen in the online version of the article showing the energy and velocity plots together with animation videos.

We finally propose to define a dimensionless parameter capable of predicting the limit between the coalescence and bouncing regimes. After the analysis presented here it is clear that the importance of the viscous forces in the gas phase

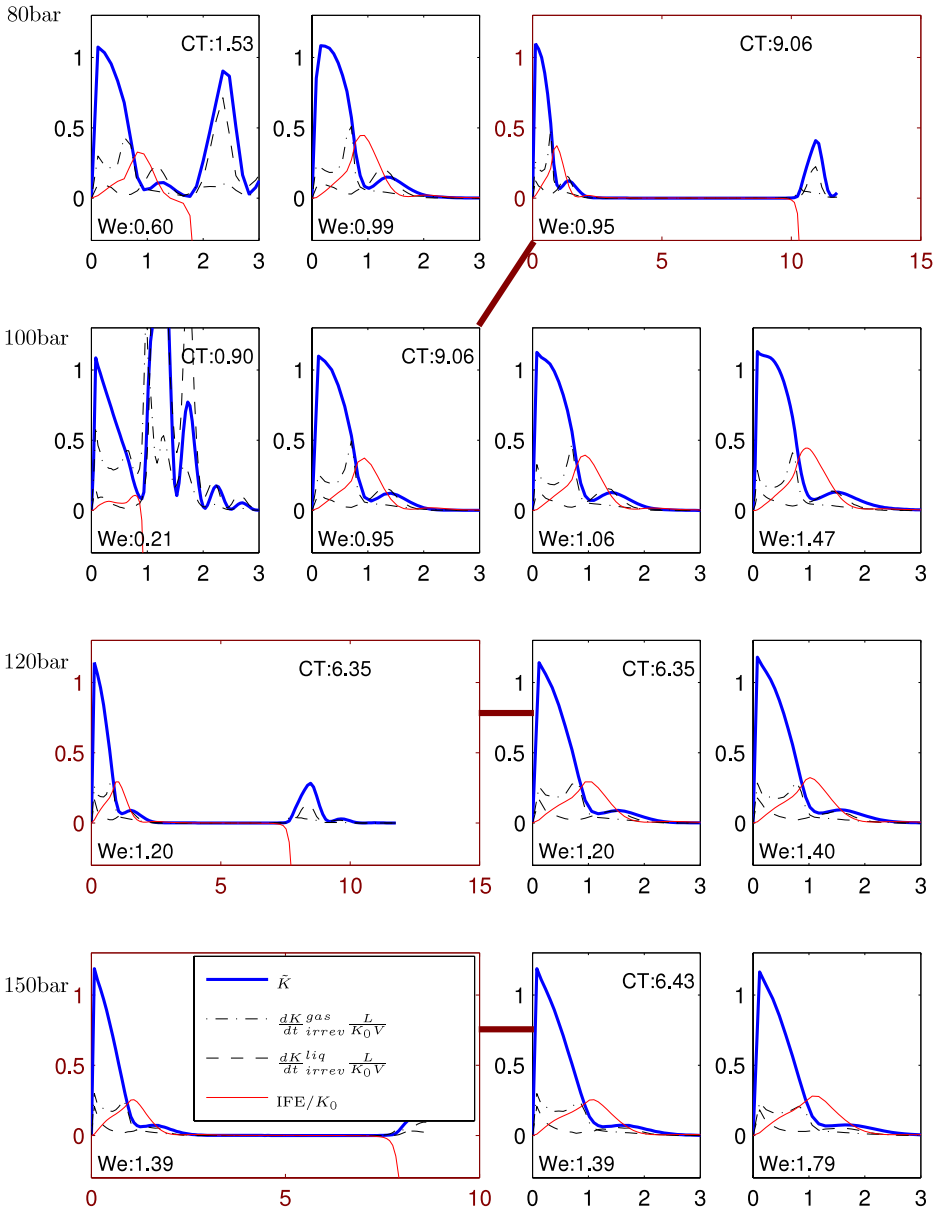

Fig. 9. Energy plot for all simulated cases ordered by ambient pressure and Weber number. The upper right-hand corner numbers correspond to the dimensionless coalescence time. Plots without this time resulted in bouncing.

cannot be neglected. For this reason we have kept the gas dynamic viscosity in the Reynolds definition in this work, defining the liquid Reynolds number as the one using the liquid viscosity. In addition, and to mark a difference for cases of higher density ratios, we propose to introduce the square root of liquid/gas property ratios as was done by Czerwonatis and Eggers [25] when modifying the Ohnesorge (Oh) number. As the simulations presented here have an almost constant viscosity ratio, additional work needs to be done to determine whether this ratio needs to be introduced. To generalize the results and plot all the cases together, the coalescence time can be used to define a quantifier for whether or not coalescence takes place. Since for bouncing cases the coalescence time is infinity, this parameter is not directly suitable. However, the inverse coalescence time (ICT), which is zero for bouncing cases, is suitable. Fig. 10 shows the ICT as a function of the different parameters. All bouncing cases are plotted as null coalescence speed. For all the head-on cases examined at different pressures, simulations with $Re > 170\sqrt{\rho_{lg}}$ resulted in bouncing. In Fig. 10 it can be seen that the definition of the Reynolds number cannot be used by itself, and neither can that of the Weber number. The most recent work grouping droplet collisions [26] proposes an empirical correlation for high inertia cases based on $We^{0.92}Oh^{0.57}$, which, as can be seen in Fig. 10, is not useful under our conditions. The data are aligned for the Reynolds number multiplied by the density ratio, and the limit between bouncing and coalescence can be easily identified. Thus the proposed parameter is $\mathrm{Re}_{\sqrt{gl}} = \sqrt{\rho_g \rho_l}\frac{uD}{\mu}$.

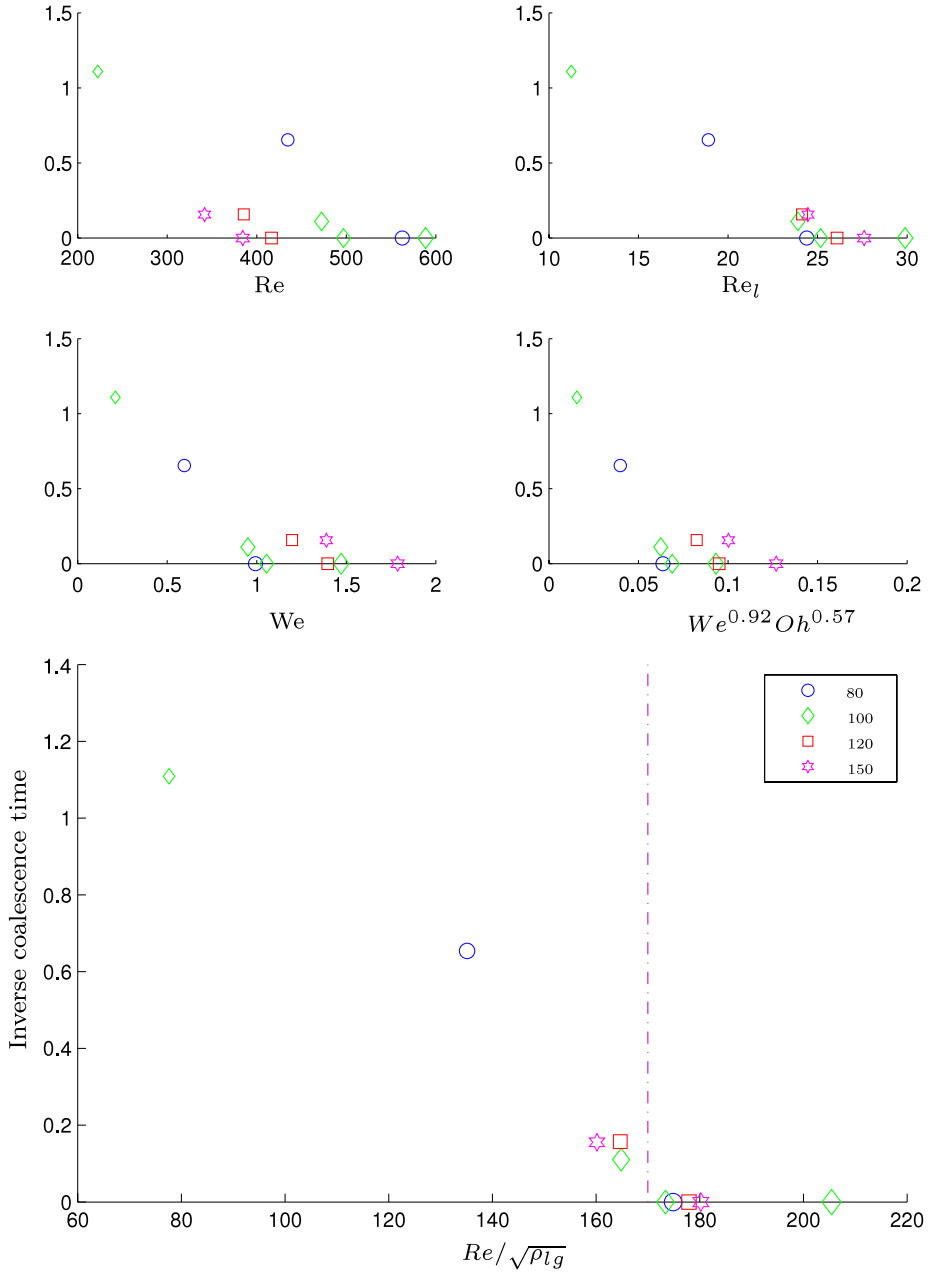

Fig. 10. Inverse of the coalescence time as a function of different parameters. The box inset gives the symbols for pressures: 80 bar, 100 bar, 120 bar and 150 bar.

7. Conclusion and recommendations for further work

Binary head-on droplet collisions at high pressure have been simulated. The results allowed us to describe the process in terms of energy and hydrodynamic variables. This quantitative study of energy loss is a way of seeking clear explanations of and insights into collision mechanisms. The energy analysis gives us insight about which phenomena are more relevant and how they can be used for defining new boundaries when building collision maps. We have shown that the principal phenomena governing respectively high pressure, low inertia and low pressure, high inertia collisions are different. This suggests that the traditional Weber number description is of less value under these conditions, and that a modified Re description could be adopted.

A more detailed description of the process of low Weber number coalescence (or secondary coalescence) [2] was given by numerical simulations. All the collision outcomes were compared by means of an inverse coalescence time. The

borders between the coalescence and bouncing regimes could be identified by $\mathrm{Re} = 170\sqrt{\rho_{lg}}$ in the absence of external perturbations. In real applications at high pressure more stochastic behaviour is expected.

The present study gives the results of collisions between two-dimensional droplets. We believe that the qualitative study and the general trends can be extrapolated to real cases of three-dimensional droplets. Furthermore, the interfaces present in this paper are thicker than they should be compared to the size of the droplets. This characteristic has a notable influence on the collision outcome, and in the authors' opinion these aspects should be improved in future work. A case with larger droplet sizes relative to interface thickness can be achieved by simple local mesh refinement or by multi-scale multi-model coupling at the interfaces [27]. Nevertheless, the conclusions drawn for the simulations at different pressures, like the energy analysis, together with the definition of the modified Reynolds number, are useful for clarifying the phenomena governing high pressure droplet collisions.

Appendix. Supplementary data

Supplementary data associated with this article can be found, in the online version, at doi:10.1016/j.camwa.2010.05.044.

References

[1] N. Ashgriz, J. Poo, Coalescence and separation in binary collisions of liquid drops, Journal of Fluid Mechanics 221 (1990) 183–204.
[2] J. Qian, C. Law, Regimes of coalescence and separation in droplet collision, Journal of Fluid Mechanics 331 (1997) 59–80.
[3] C. Gotaas, P. Havelka, H.A. Jakobsen, H.F. Svendsen, M. Hase, N. Roth, B. Weigand, Effect of viscosity on droplet–droplet collision outcome: experimental study and numerical comparison, Physics of Fluids 19 (10) (2007) 102106. doi:10.1063/1.2781603.
[4] P.M. Dupuy, M. Fernandino, H.A. Jakobsen, H.F. Svendsen, Fractional step two-phase flow lattice Boltzmann model implementation, Journal of Statistical Mechanics: Theory and Experiment (2009) P06014. doi:10.1088/1742-5468/2009/06/P06014.
[5] A. Gunstensen, D. Rothman, S. Zaleski, G. Zanetti, A discrete Boltzmann equation model for non-ideal gases, Physical Review A 43 (1991) 4320–4327.
[6] X. Shan, H. Chen, Lattice Boltzmann model for simulating flows with multiple phases and components, Physical Review E 47 (3) (1993) 1815–1819. doi:10.1103/PhysRevE.47.1815.
[7] X. Shan, X.-F. Yuan, H. Chen, Kinetic theory representation of hydrodynamics: a way beyond the Navier–Stokes equation, Journal of Computational Physics 550 (2006) 413–441.
[8] M.R. Swift, W.R. Osborn, J.M. Yeomans, Lattice Boltzmann simulation of nonideal fluids, Physical Review Letters 75 (5) (1995) 830–833. doi:10.1103/PhysRevLett.75.830.
[9] M. Swift, E. Orlandini, W. Osborn, J. Yeomans, Lattice Boltzmann simulations of liquid–gas and binary fluid systems, Physical Review E 54 (1996) 5041–5052.
[10] N.S. Martys, H. Chen, Simulation of multicomponent fluids in complex three-dimensional geometries by the lattice Boltzmann method, Physical Review E 53 (1) (1996) 743–750. doi:10.1103/PhysRevE.53.743.
[11] X. He, S. Chen, R. Zhang, A lattice Boltzmann scheme for incompressible multiphase flow and its application in simulation of Rayleigh–Taylor instability, Journal of Computational Physics 152 (2) (1999) 642–663. doi:10.1006/jcph.1999.6257.
[12] X. He, R. Zhang, S. Chen, G.D. Doolen, On the three-dimensional Rayleigh–Taylor instability, Physics of Fluids 11 (5) (1999) 1143–1152.
[13] R. Zhang, X. He, S. Chen, Interface and surface tension in incompressible lattice Boltzmann multiphase model, Computer Physics Communications 129 (1–3) (2000) 121–130. doi:10.1016/S0010-4655(00)00099-0.
[14] R. Zhang, X. He, G. Doolen, S. Chen, Surface tension effects on two-dimensional two-phase Kelvin–Helmholtz instabilities, in: Pore Scale Modeling, Advances in Water Resources 24 (3–4) (2001) 461–478. doi:10.1016/S0309-1708(00)00067-1.
[15] B.B. Hamel, Kinetic model for binary gas mixtures, Physics of Fluids 8 (3) (1965) 418–425. doi:10.1063/1.1761239.
[16] L.-S. Luo, S.S. Girimaji, Theory of the lattice Boltzmann method: two-fluid model for binary mixtures, Physical Review E 67 (3) (2003) 036302. doi:10.1103/PhysRevE.67.036302.
[17] P. Asinari, Asymptotic analysis of multiple-relaxation-time lattice Boltzmann schemes for mixture modeling, Computers and Mathematics with Applications 55 (7) (2008) 1392–1407. doi:10.1016/j.camwa.2007.08.006.
[18] P.M. Dupuy, M. Fernandino, H.A. Jakobsen, H.F. Svendsen, Using Cahn–Hilliard mobility to simulate coalescence dynamics, Computers and Mathematics with Applications 59 (2010) 2246–2259. doi:10.1016/j.camwa.2009.08.050.
[19] J. Cahn, J. Hilliard, Spinodal decomposition: a reprise, Acta Metallurgica 19 (1971) 151–161.
[20] J.W. Cahn, J.E. Hilliard, Free energy of a nonuniform system. I. Interfacial free energy, The Journal of Chemical Physics 28 (2) (1958) 258–267. doi:10.1063/1.1744102.
[21] C. Shu, X.D. Niu, Y.T. Chew, Q.D. Cai, A fractional step lattice Boltzmann method for simulating high Reynolds number flows, Mathematics and Computers in Simulation 72 (2–6) (2006) 201–205. doi:10.1016/j.matcom.2006.05.014.
[22] T. Lee, C.-L. Lin, A stable discretization of the lattice Boltzmann equation for simulation of incompressible two-phase flows at high density ratio, Journal of Computational Physics 206 (1) (2005) 16–47. doi:10.1016/j.jcp.2004.12.001.
[23] H.A. Jakobsen, Chemical Reactor Modeling. Multiphase Reactive Flows, Springer, 2008.
[24] G.A. Bach, D.L. Koch, A. Gopinath, Coalescence and bouncing of small aerosol droplets, Journal of Fluid Mechanics 518 (1) (2004) 157–185. doi:10.1017/S0022112004000928.
[25] N. Czerwonatis, R. Eggers, Disintegration of liquid jets and drop drag coefficients in pressurized nitrogen and carbon dioxide, Chemical Engineering and Technology 24 (2001) 619–624.
[26] C. Rabe, J. Malet, F. Feuillebois, On the influence of droplet coalescence in spray systems for containment safety, in: The 13th International Topical Meeting on Nuclear Reactor Thermal Hydraulics, 2009.
[27] P. Dupuy, M. Fernandino, H. Jakobsen, H. Svendsen, Multiphysics two-phase flow lattice Boltzmann: droplets with realistic representation of the interface, Communications in Computational Physics, (2010) (submitted for publication).